




Science Forum (Journal of Pure and Applied Sciences)

journal homepage: <https://atbu.edu.ng/science-forum/>



Antibacterial potentials of silver nanoparticles synthesized from *Calopogonium mucunoides* leaves extract on some enteric bacteria

Abdulameen Saheed Adedeji^{1*} , Nasiru Usman Adabara¹, Jimoh Oladejo Tijani², Sherifat Ozavize Enejiyon¹, Fawziyyah Usman Sadiq³, Aisha Usman⁴, Faruk Adamu

¹Department of Microbiology, Faculty of Life Sciences, Federal University of Technology, Minna, Nigeria

²Department of Chemistry, Faculty of Physical Sciences, Federal University of Technology, Minna, Nigeria

³Department of Microbiology, Faculty of Natural and Applied Sciences, Nile University, Abuja, Nigeria

⁴Department of Microbiology, Faculty of Science, Kaduna State University, Kaduna, Nigeria



ABSTRACT

Silver nanoparticles (AgNPs) synthesized from *Calopogonium mucunoides* aqueous leaf extract and determination of the antibacterial activities against selected enteric bacteria were conducted in this study. The AgNPs were produced in an eco-friendly manner by combining a 1 mM silver nitrate solution with an aqueous *C. mucunoides* leaf extract under direct sunshine. UV-visible spectrophotometry, dynamic light scattering (DLS), and high-resolution transmission electron microscopy (HRTEM) were utilized to study the AgNPs (HRTEM). AgNPs were brown in colour and had a UV-Vis absorbance peak at 441–445 nm. DLS uncovered monodispersed AgNPs with an 80.77 nm hydrodynamic diameter. A HRTEM image revealed that AgNPs with an average size of 7.5 nm had a spherical morphology. The antimicrobial susceptibility of colloidal AgNPs (50, 75, 100, and 150 µg/ mL) utilizing agar diffusion techniques against bacterial isolates (*Pseudomonas aeruginosa* strain DM1, *Salmonella typhi* strain T8, and *Escherichia coli* Acj 213) revealed inhibition zones ranging from 16.70 to 21.00 mm. For three bacterial isolates, the lowest inhibitory concentrations were 37.50, 37.50, and 9.38 µg/mL, and the minimum bactericidal values were 75, 75, and 37.5 µg/mL, respectively. The outcomes of this study indicate that the aqueous leaf extract of *C. mucunoides* can be used to synthesize AgNPs with a considerable anti-bacterial impact against clinical isolates of *P. aeruginosa* strain DM1, *S. typhi* strain T8, and *E. coli* Acj 213. To assure the safety of biogenic AgNPs for the development of novel antimicrobial drugs, additional research is needed to assess their toxicity.

ARTICLE INFO

Article history:

Received 17 January 2023 Received in

revised form 18 January 2023

Accepted 19 January 2023

Published 30 October 2023

Available online: 30 October 2023

KEYWORDS

Calopogonium mucunoides

Biogenic

Micrograph

X-ray diffraction

1. Introduction

Antibiotic treatment of bacterial infections is becoming increasingly difficult to sustain due to the increased emergence and re-emergence of multi-drug resistant pathogens (Taylor et al., 2005). In pursuit of innovative treatment, there is a growing interest in the

use of nanomaterials with antibacterial potentials to combat the menace of pathogens because microbes find it extremely difficult to acquire resistance toward nanoparticles as they target multiple bacterial components, contrary to the mechanistic action of conventional antibiotics (Dhanalekshmi and Meena, 2014).

* Corresponding author Abdulameen Saheed Adedeji ✉ sabdulameen@futminna.edu.ng ✉ Department of Microbiology, Faculty of Life Sciences, Federal University of Technology, Minna, Nigeria.

Nanoparticles are materials with at least one dimension in the range of 1–100 nm that can be manufactured using a variety of methods, including chemical, physical, and biological (Kumar et al., 2013; Shah et al., 2013). The chemical technique uses chemical compounds with reducing and stabilizing potentials to decrease metallic ions into nanosized particles. These compounds may cause surface contamination and the introduction of structural flaws, jeopardizing their use (Kumar et al., 2013). Laser ablation in a liquid media, high-energy ball milling, and spraying are all part of the physical approach. Despite the fact that they are not chemically harmful, they demand high temperatures and pressures, which take a lot of energy (Kumar et al., 2013; Patil et al., 2016). Because of the drawbacks of the chemical and physical methodologies, there is a growing interest in the biological approach to the production of metallic nanoparticles. The method is deemed non-hazardous, cost-effective, and most importantly, environmentally benign because pricey chemicals are replaced with plant extracts or microorganisms (Rao and Paria, 2013). Plant extract-mediated synthesis, in particular, offers considerable promise, as the extracts readily cap and stabilize the nanoparticles.

Plant extracts contain enzymes (reductases, hydrogenases) and phytochemicals such as terpenoids, flavonoids, and phenolic compounds, which act as bioreductants and capping agents in the presence of metal salts for nanoparticle production (Rao and Paria, 2013). *Calopogonium mucunoides* is a strongly spreading, hairy, annual trailing legume with a long history of use in Nigerian folk medicine (Borokini and Omotayo, 2010). It has long been used to treat ulcers, diarrhea, and a variety of other bacterial illnesses, and it has been shown to be high in bioactive chemicals (Borokini and Omotayo, 2010). To the best of our knowledge, *C. mucunoides* has not been used in the synthesis of silver nanoparticles (AgNPs). As a result, the goals of this research are to synthesize AgNPs from an aqueous plant extract of *C. mucunoides* and then test their antibacterial effectiveness against specific bacterial pathogens.

2. Material and Methods

2.1. Collection of plant materials

Calopogonium mucunoides leaves were collected from various sites on the Federal University of Technology, Minna's Bosso campus. At the Department of Plant Biology, Federal University of Technology, Minna, the plant was identified and given a voucher number (CA

458BS). The voucher was thereafter deposited in the herbarium of the Department.

2.2. Preparation of the plant extract

Calopogonium mucunoides leaves were cleaned with distilled water and air dried for 7 days at room temperature. Using an electronic blender, the plant leaves were ground into a fine powder.

Extracts of varying strengths (1%, 5%, and 10%) were made by dissolving different quantities (1, 5, and 10 g) of powdered leaves in 100 mL of distilled water in a conical flask separately for 30 minutes in a water bath at 60°C under vigorous shaking. The crude extracts were centrifuged at 4,000 rpm for 10 minutes before being filtered using Whatman No. 1 filter paper (pore size: 25 µm). The filtrates were employed to create the AgNPs (Devasenan et al., 2016; Nagaonkar and Rai, 2015).

2.3. Biosynthesis of AgNPs

The *C. mucunoides* leaf extracts were placed (1 mL each) into three distinct 20-mL specimen bottles containing 8, 9, and 10 mL of a 10³ M silver nitrate (Sigma Aldrich) solution. The control solution was 9 mL of a 10³ M silver nitrate solution (Das et al., 2016). The solutions that resulted were stored in direct sunlight. The results of observation for the progressive color shift were recorded. The storage impact of biosynthesized AgNPs was investigated over a 4-week period using weekly UV-Vis measurements. The characteristic spectra for AgNPs were observed for alterations or disappearance. Samples that did not exhibit the typical spectrum for AgNPs were discarded.

2.4. Characterization of synthesized nanoparticles

The synthesis of AgNPs was evaluated by determining the absorption spectra of generated AgNPs using a UV-Vis spectrophotometer. A dynamic light scattering (DLS) approach using Malvern® Zetasizer Nano ZS was used to determine the particle size distribution and polydispersity index (PDI) of the sample (Malvern Panalytical, UK). The microstructure of the AgNPs was studied using a high-resolution transmission electron microscope (HRTEM) (Carl Zeiss AG, Germany).

2.5. Test microorganisms

This study's clinical bacterial isolates were obtained from the General Hospital in Minna, Niger State. The bacterial isolates include *Escherichia coli*, *Pseudomonas aeruginosa*, and *Salmonella typhi*. These bacterial isolates are global pathogens with rising resistance

strategies, necessitating the use of innovative or novel antibacterial(s) for their effective treatment, thus the choice. The isolates were further purified and subcultured on a differential medium for 24 hours at 37°C. The isolates were molecularly identified using the approach outlined by Frank et al. (2008).

2.6. Antibacterial effect of the AgNPs

The antibacterial activity of produced colloidal AgNPs and aged AgNPs was tested *in vitro* in comparison with the standard antibiotic, Beecham Ampiclox (30 g/ml), using the agar well diffusion method (Pai et al., 2011). In 12 sterile Petri plates, 20 mL of sterilized nutritional agar were dispensed. Before inoculating, the agar was allowed to be set, and 5 mm wells were drilled on each plate with a sterile cork borer (Idu and Onyibe, 2007). The wells were then filled with 160 µL of AgNPs and aged AgNPs at various concentrations (50, 75, 100, and 150 µg) using a microtiter pipette. This was allowed to diffuse for 2 hours at ambient temperature. The plates were incubated for 24 hours at 37°C. As a control, a plant extract was employed. When a zone of inhibition was identified after the 24-hour incubation period, positive test results were recorded (Kora et al., 2009).

2.7. Determination of minimum inhibitory concentration (MIC) and minimum bactericidal concentration (MBC) of AgNPs

The AgNPs' MIC and MBC were determined as follows: using 2 mL of nourishing broth in six test tubes, the colloidal AgNPs were serially diluted to acquire different concentrations (150, 75, 37.5, 18.75, 9.375, and 4.6875 µg/mL). The tubes were inoculated with 0.2 mL of standardized bacterial isolate inoculum. The tubes were incubated at 37°C overnight. Positive controls were tubes holding broth and AgNPs without inoculum, while negative controls were tubes containing broth plus inoculum (Matai et al., 2014).

Visual observation was used to determine the growth of cultures. The MIC value was assigned to the culture tube with the lowest concentration of AgNPs that showed no growth, while the MBC value was assigned to the tube that lacked turbidity. The MBC value was defined as the lowest concentration of AgNPs that inhibited bacterial cell growth upon re-inoculation in Muller-Hinton agar (Matai et al., 2014).

3. Results

3.1. Biosynthesis of AgNPs

The mixture of 1 mM colorless AgNO₃ solution with 1%, 5%, and 10% *C. mucunoides* aqueous leaf extract

in the ratios 1:8, 1:9, and 1:10 produced a stable brown color within 10 minutes under solar irradiation (Plate I), an indication of the formation of AgNPs.

3.2. UV-Vis absorption spectrum of AgNPs

The aqueous leaf extract of *C. mucunoides* reacted with 1 mM AgNO₃ in the ratios 1:8 (S1-8) and 1:9 (S1-9) to indicate the presence of a prominent and broad surface plasmon resonance (SPR) peak at 441 and 439 nm which depicts AgNP production. While no SPR peak was detected for 1:10 (S1-10) (Fig. 1a).

Similarly, the UV-Vis absorption spectra of AgNPs from 5% *C. mucunoides* aqueous leaf extract reacted with 1 mM AgNO₃ in the ratios 1:8 (S2-8), 1:9 (S2-9), and 1:10 (S2-10), revealing a more pronounced SPR peak at 442, 440, and 441 nm, confirming the presence of AgNPs (Fig. 1b).

Furthermore, the UV-Vis absorption spectrum of AgNPs obtained for 10% *C. mucunoides* aqueous leaf extract reacted with 1 mM AgNO₃ of the same ratios exhibited an intense SPR peak at 438 for 1:8 (S3-8) but the most intense peak at 440 was obtained for ratio 1:9 (S3-9) and hence these AgNPs were regarded as the best and therefore selected for further studies (Fig. 1c).

The UV-Vis absorption spectra of S3-9 AgNPs revealed a strong and broad SPR peak at 440 for S3-9. While AgNO₃ showed a SPR peak at 211 nm (Fig. 1d). UV-Vis absorption spectrum of distinctive S3-9 AgNPs and 1 mM AgNO₃ (Fig. 1d).

Out of the seven colloidal AgNPs (S1-8), (S1-9), (S2-8), (S2-9), (S2-10), (S3-8), and (S3-9) stored

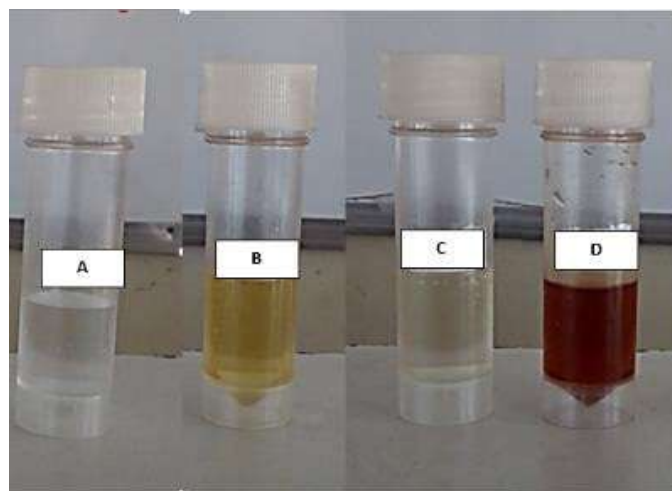


Plate I. Biosynthesis of AgNPs using aqueous leaf extract of *C. mucunoides*. A = 1 mM AgNO₃ solution; B = Plant extract; C = 1 mM AgNO₃ solution + Plant extract at zero minute; D = Colloidal AgNPs after 10 minutes.

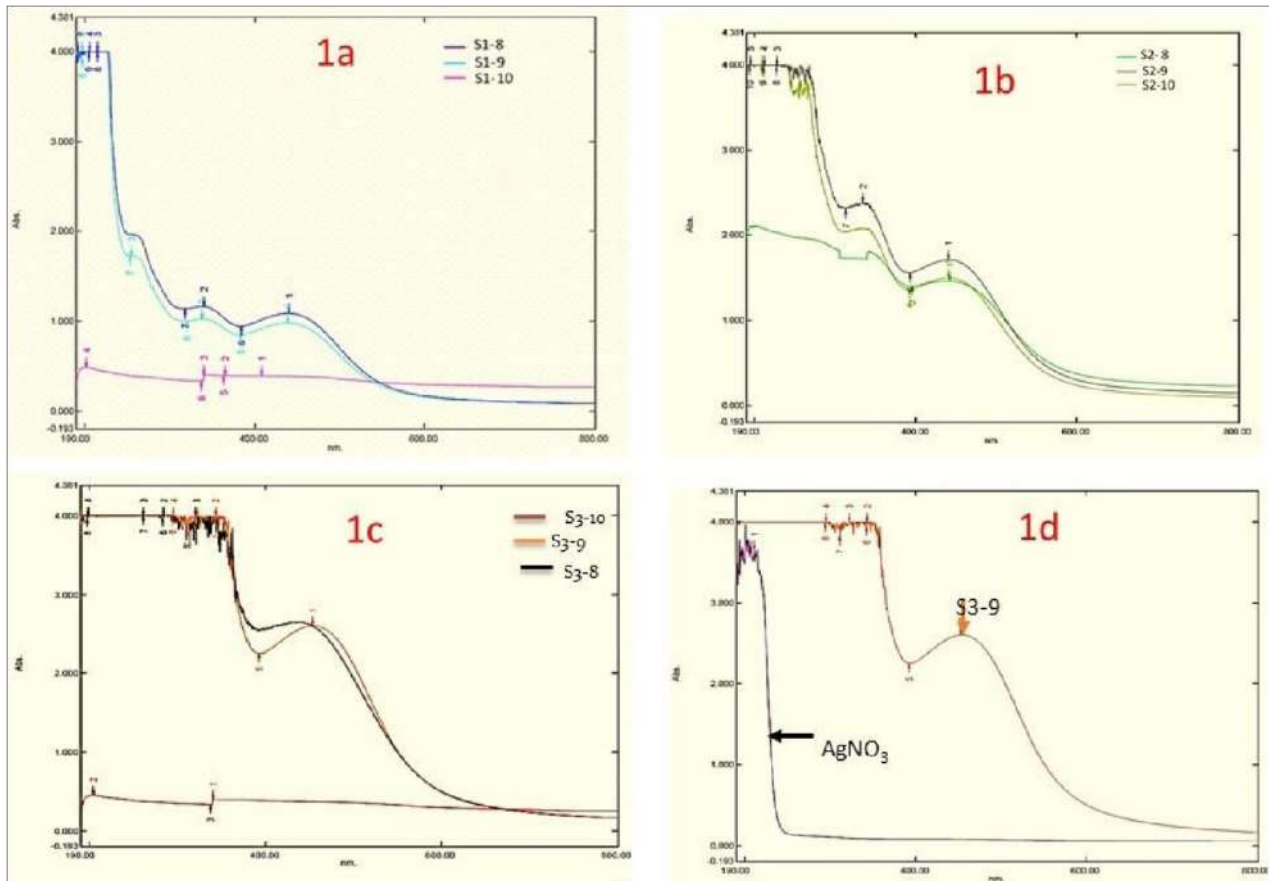


Figure 1. (a–c) UV-Vis absorption spectrum of colloidal 1%, 5%, and 10% AgNPs. (d) UV-Vis absorption spectrum of distinctive S3–9 AgNPs and 1 mM AgNO₃.

under ambient conditions, only (S1–9) AgNPs became more intense and sharper with increasing shelf life (Fig. 2).

3.3. Particle size distribution measurement

The particle size distribution profile of the S3–9 AgNPs was determined by DLS (Fig. 3). The hydrodynamic diameter of the biosynthesized AgNPs was found to be 80.77 nm. The PDI was 0.178.

3.4. TEM and Surface area electron diffraction (SAED) analysis

The HRTEM micrograph revealed the formation of partially distributed spherical particles with an average size of approximately 7.5 nm (Plate IA–C). The SAED patterns of the AgNPs show clear circular rings, which suggest the polycrystalline nature of the AgNPs. The presence of lattice fringes in TEM images indicates that AgNPs are highly crystalline (Plate II).

3.5. Zones of inhibition (mm) produced by colloidal S3–9 AgNPs

The colloidal S3–9 AgNPs at 50–150 µg/mL showed appreciable antibacterial activity with zones of inhibition ranging from 17–21 mm on *S. typhi* strain T8,

E. coli strain Acj 213, and *P. aeruginosa* strain DM1 (Table 1).

3.6. MIC and MBC of colloidal S3–9 AgNPs

The MIC of colloidal S3–9 AgNPs was 37.50, 37.50, and 9.38 µg/mL, respectively, while the MBC values were 75.00, 75.00, and 37.50 µg/ml for *S. typhi* strain T8, *E. coli* Acj 213, and *P. aeruginosa* strain DM1, respectively (Table 2).

3.7. Antimicrobial effect of 1 month aged colloidal S1–9 AgNPs

The biosynthesized S1–9 AgNPs showed antibacterial activities at a –150 µg/mL with zones of inhibition ranging from 14–20 mm on *S. typhi* strain T8, *E. coli* Acj 213, and *P. aeruginosa* strain DM1, after 1 month of synthesis (Table 3).

4. Discussion

AgNPs were generated in this study by reducing aqueous silver ions under the impact of sunshine irradiation using *C. mucunoides* aqueous leaf extract. Under solar irradiation, a mixture of 1 mM colorless AgNO₃

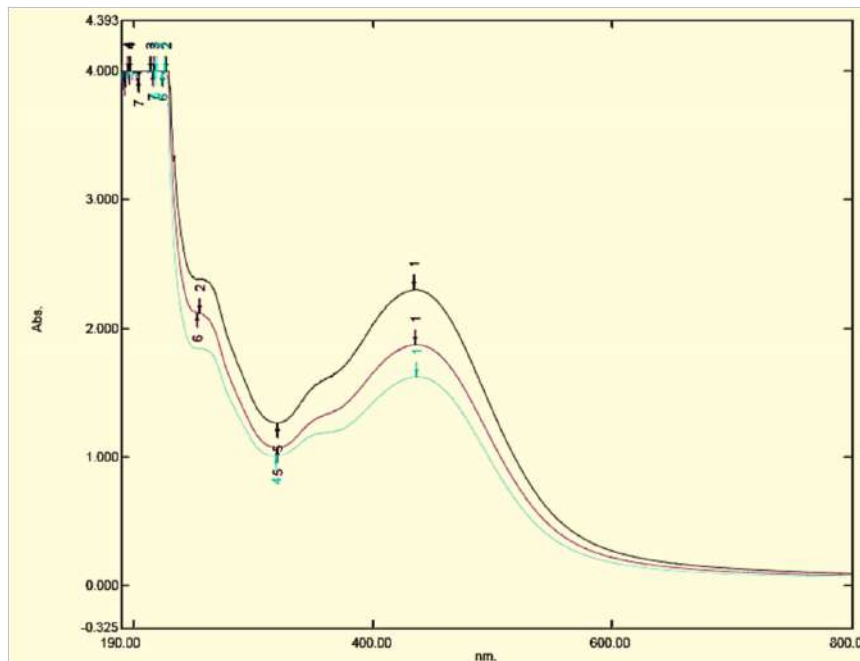


Figure 2. UV-Vis absorption spectrum of S1–9 AgNPs over 1 month.

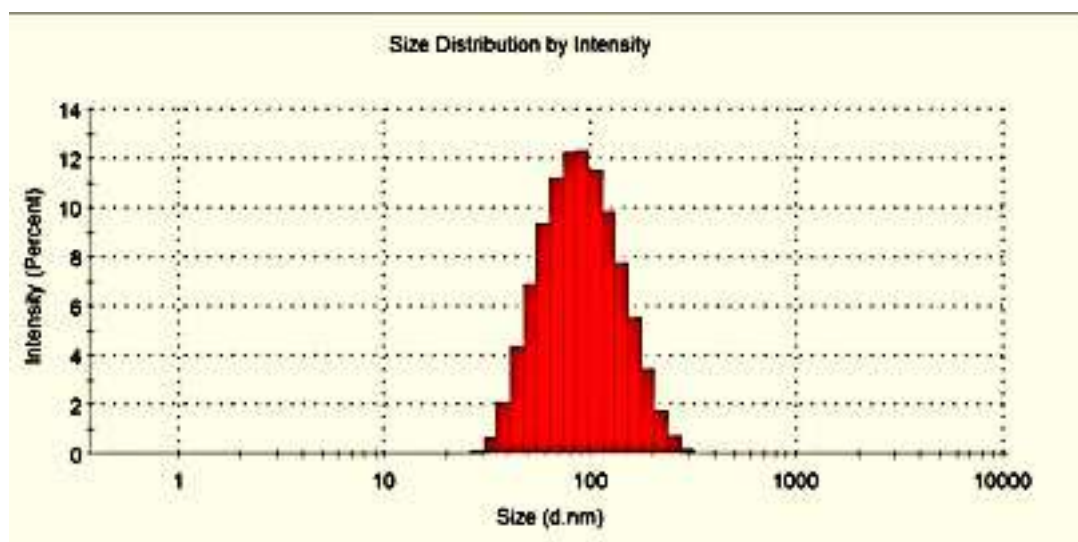


Figure 3. DLS measurement of S3–9 AgNPs.

solution with 1%, 5%, and 10% *C. mucunoides* aqueous leaf extract in the ratios 1:8, 1:9, and 1:10 generated a persistent brown color within 10 minutes, indicating the synthesis of AgNPs (Plate I). The excitation of surface plasmon vibrations in metal nanoparticles causes these color formations (Jayaramudu et al., 2016). The protocols utilized in this investigation are consistent with those published by Jayaramudu et al. (2016) and Abbasi et al. (2017), making this study compared to earlier research.

The stimulation of the surface plasma resonance of the produced AgNPs led to the UV-visible absorption spectra revealed (Fig. 1a–e). It was noted that

the extracts' concentration rise favored the production of AgNPs. However, it is not clear from this study why the observations in S1–10 and S3–10 were made. It is possible that the creation of sizable anisotropic particles is what causes the broad SPR peaks at lower *C. mucunoides* concentrations. This suggests that the amount of phytochemicals such as phenolics, alkaloids, tannins, flavonoids, and sugars that could have aided in the bioreduction of Ag⁺ ions to metallic AgNPs was decreased at a low concentration of aqueous leaf extract from *C. mucunoides*. Similar SPR peaks for biosynthesized AgNPs have been found in several

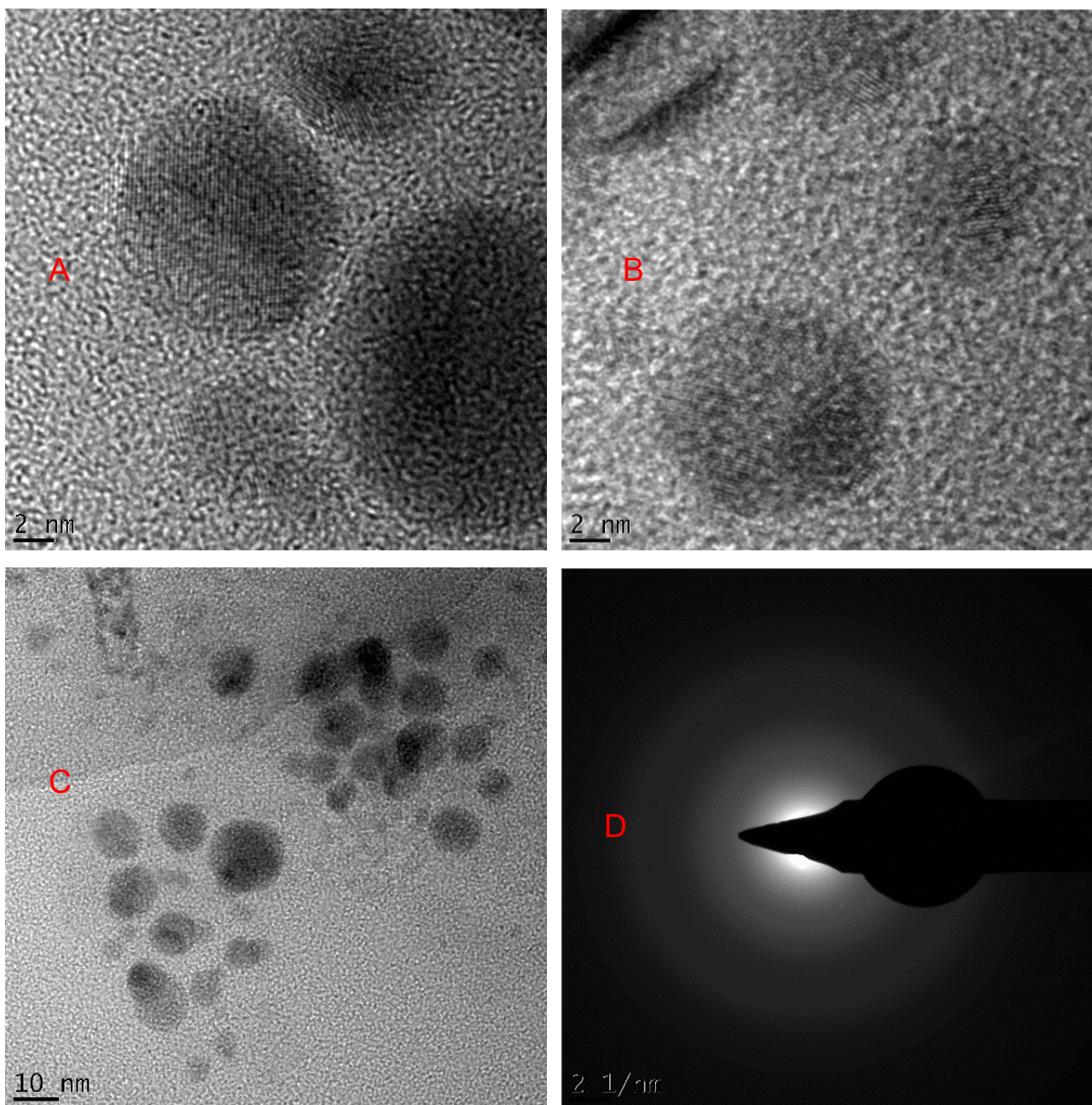


Plate II. (A–C) TEM images of the PEG conjugated S3–9 AgNPs and (D) SAED pattern.

Table 1. Zones of inhibition (mm) produced by colloidal S3–9 AgNPs.

Concentration of AgNPs ($\mu\text{g/mL}$)	<i>S. typhi</i> strain T8	<i>P. aeruginosa</i> strain DM1	<i>E. coli</i> Acj 213
50	17.7 ± 1.52^b	20.3 ± 3.79^a	16.7 ± 1.52^b
75	19.0 ± 1.00^b	20.6 ± 2.31^a	17.7 ± 1.52^b
100	18.7 ± 1.15^b	20.0 ± 1.73^a	17.7 ± 1.52^b
150	19.3 ± 1.52^b	21.0 ± 2.65^a	17.3 ± 2.08^b
Control (30)	39.0 ± 0.00^a	24.0 ± 0.00^a	30.0 ± 0.00^a

Values are in mean \pm standard deviation of triplicate determinations.

Means with the same letter in a column do not differ significantly according to Duncan's Multiple Range Test (DMRT) at $p = 0.05$.

investigations (Amin et al., 2012; Shahverdi et al., 2007; Vigneshwaran et al., 2007).

S3–9 AgNPs' absorption peak is the sharpest and most intense, according to a comparison of the absorption peaks produced at various reaction volumes and extract concentrations. The peak's sharpness reveals the creation of stable isotropic particles (AgNPs), while the intensity measures the amount of nanosilver created (Nanocomposix, 2015). As a result, S3–9 AgNPs were chosen for characterization, antibacterial research, and toxicity testing in Wistar rats since they were thought to be the best.

Furthermore, colloidal particle stability is now analyzed quantitatively using UV-Vis spectroscopy (Nanocomposix, 2012). If the colloidal particles are not stable, the initial absorption peak will diminish, vanish, broaden, and/or appear at a longer wavelength as a result of aggregate formation (Nanocomposix, 2015). This was true for the nanosilver colloids S1–8, S2–8, S2–9, S2–10, S3–8, and S3–9 which were put on hold for 4 weeks. However, –compared to another sample that was shelved, the S1–9's UV-Vis absorption spectrum improved over the course of a month, showing a beneficial age impact (Fig. 2). The creation of highly stable and isotropic AgNPs may be caused by giving the biosynthesized AgNPs more time to interact with phytochemicals that weren't involved in the reduction of silver ions (i.e., capping agents).

DLS is a technique used to determine the size, size distribution profile, and PDI of particles in a colloidal suspension (Nanocomposix, 2015). PDI values greater than 0.5 indicate particle aggregation (Nanocomposix, 2015), indicating that the AgNPs in this study are monodispersed and did not aggregate in colloidal solution, as evidenced by the HRTEM micrographs in Plate III.

Table 2. MIC and MBC of colloidal S3–9 AgNPs.

Isolates	MIC ($\mu\text{g}/\text{mL}$)	MBC ($\mu\text{g}/\text{mL}$)
<i>S. typhi</i> strain T8	37.5 \pm 1.52	75 \pm 0.70
<i>E. coli</i> Acj 213	37.5 \pm 0.00	75 \pm 0.02
<i>P. aeruginosa</i> strain DM1	37.5 \pm 0.00	9.38 \pm 0.71

Values are in mean \pm standard deviation of triplicate determinations.

Means with the same letter in a column do not differ significantly according to Duncan's Multiple Range Test (DMRT) at $p = 0.05$.

Table 3. Zones of inhibition (mm) produced aged colloidal S1–9 AgNPs.

Concentration of AgNPs ($\mu\text{g}/\text{mL}$)	<i>S. typhi</i> strain T8	<i>P. aeruginosa</i> strain DM1	<i>E. coli</i> Acj 213
50	14.5 \pm 0.70 ^b	17.0 \pm 1.41 ^c	15.5 \pm 0.71 ^d
75	16.0 \pm 0.00 ^b	14.5 \pm 0.71 ^b	17.0 \pm 0.00 ^c
100	17.0 \pm 0.00 ^b	20.5 \pm 0.71 ^b	17.0 \pm 1.41 ^c
150	18.5 \pm 0.00 ^b	20.0 \pm 0.00 ^b	18.5 \pm 0.71 ^b
Control (30)	39.0 \pm 0.00 ^a	24.0 \pm 0.00 ^a	30.0 \pm 0.00 ^a

Values are in mean \pm standard deviation of triplicate determinations.

Means with the same letter in a column do not differ significantly according to Duncan's Multiple Range Test (DMRT) at $p = 0.05$.

S3–9 AgNPs are spherical in shape and well scattered, as seen in HRTEM micrograph Plates IA–C. This corresponds to DLS particle size distribution data (Fig. 3). The S3–9 AgNPs crystals have a diameter of about 7.5 nm. The difference in diameter revealed by TEM and DLS data is not surprising, and it could be related to the presence of capping agents (such as ions or molecules that stabilized AgNPs), which have the capacity to offset the diameter of AgNPs in colloids. The existence of lattice fringes (parallel lines in the TEM pictures) confirms the X-Ray diffraction analysis (XRD) findings and suggests that the biosynthesized S3–9 AgNPs were crystalline in form.

The crystallinity of the S3–9 AgNPs with a distinct circular ring is further supported by the SAED pattern of the biosynthesized AgNPs (Plate II–D).

Antibacterial activity of AgNPs produced at 50, 75, 100, and 150 $\mu\text{g}/\text{mL}$ utilizing agar diffusion techniques against clinical strains of *S. typhi* strain T8, *P. aeruginosa* strain DM1, and *E. coli* Acj 213. The inhibition zones obtained ranged from 16.70 to 21.00 mm. The results showed that *P. aeruginosa* strain DM1 was the most susceptible, with a 21 mm inhibition zone diameter at 150 $\mu\text{g}/\text{mL}$, while *E. coli* Acj 213 had the smallest (16.70 mm) at 50 $\mu\text{g}/\text{mL}$ (Table 1). It was expected that variations in concentration would produce different results due to their levels of potency. However, no significant differences ($p > 0.05$) were seen between concentrations for the three test isolates. When compared to the biosynthesized AgNPs, the control antibiotic exhibited considerably greater inhibitory zones against *S. typhi* strain T8 and *E. coli* Acj 213. The fact that the colloidal nanosilver contains extraneous material that could inhibit its activity makes their antibacterial effects comparable. However, the antibacterial efficacy of AgNPs against *P. aeruginosa* strain DM1 at all concentrations compared favorably with the control drug.

Similarly, a month-old colloidal S1–9 AgNPs at 50–150 $\mu\text{g}/\text{mL}$ showed excellent antibacterial activity against *S. typhi* strain T8, *P. aeruginosa* strain DM1, and *E. coli* Acj 213. This study shows that colloidal AgNPs not only remain stable in suspension but also retain their antibacterial characteristics. Again, the

correlation between increased antibacterial activity and concentration was not significant at $p < 0.05$ (Table 3). The antibacterial activity of S3–9 AgNPs is consistent with previous reports by Jyoti et al. (2016), Dama et al. (2016), Kayalvizhi et al. (2016), and Beg et al. (2017), who attribute AgNPs' antibacterial activities to their unique physicochemical properties such as their large surface area to volume ratio, shape, and size.

The variation in inhibition zones seen in this investigation and other publications (Beg et al., 2017; Dama et al., 2016; Jyoti et al., 2016; Kayalvizhi et al., 2016) could be attributed to differences in the morphology and aggregation state of the AgNPs investigated.

5. Conclusion

A unique method for producing AgNPs from an aqueous leaf extract of *C. mucunoides* has been developed. The biosynthesized AgNPs exhibited remarkable antibacterial activity, making the study a great success in the treatment of enteric bacterial infections. As a result, AgNPs should be standardized, developed into a cost-effective and acceptable drug, and/or coupled with current drugs to improve their efficacy.

References

- Abbasi Z, Feizi S, Taghipour E, Ghadam P. Green synthesis of silver nanoparticles using aqueous extract of dried *Juglans regia* green husk and examination of its biological properties. *Green Process Synth* 2017; (5):477–85.
- Amin M, Anwar F, Janjua, MRSA, Iqbal MA, Rashid U. Green synthesis of silver nanoparticles through reduction with *Solanum xanthocarpum* L. berry extract: characterization, antimicrobial and urease inhibitory activities against *Helicobacter pylori*. *Int J Mol Sci* 2012; 13(8):9923–41.
- Beg M, Maji A, Mandal AK, Das S, Aktara MN, Jha PK, et al. Green synthesis of silver nanoparticles using *Pongamia pinnata* seed: characterization, antibacterial property, and spectroscopic investigation of interaction with human serum albumin. *J Mol Recognit* 2017; 30(1):55–76.
- Borokini TI, Omotayo FO. Phytochemical and ethnobotanical study of some selected medicinal plants from Nigeria. *J Med Plant Res* 2010; (7):1106–18.
- Dama LB, Mane PP, Pathan AV, Chandarki MS, Sonawane SR, Dama SB, et al. Green synthesis of silver nanoparticles using leaf extract of *Lawsonia inermis* and *Psidium guajava* and evaluation of their antibacterial activity. *Sci Res Rep* 2016; (2):89–95.
- Das AJ, Kumar R, Goutam SP, Sagar SS. Sunlight irradiation induced synthesis of silver nanoparticles using glycolipid bio-surfactant and exploring the antibacterial activity. *J Bioeng Biomed Sci* 2016; (208):2–10.
- Devasenan S, Beev NH, Jayanthi SS. Synthesis and characterization of copper nanoparticles using leaf extract of *Andrographis paniculata* and their antimicrobial activities. *Int J Chem Tech Res* 2016; 9(04):725–30.
- Dhanalekshmi KI, Meena KS. Comparison of antibacterial activities of Ag@ TiO₂ and Ag@ SiO₂ core-shell nanoparticles. *Spectrochim Int J Nanotechnol Appl* 2014; 128:887–90.
- Frank JA, Reich CI, Sharma S, Weisbaum JS, Wilson BA, Olsen GJ. Critical evaluation of two primers commonly used for amplification of bacterial 16S rRNA genes. *Appl Environ Microbiol* 2008; 74(8):2461–70.
- Idu M, Onyibe HI. Medicinal plants of Edo State, Nigeria. *Res J Med Plant* 2007; (2):32–41.
- Jayaramudu T, Raghavendra GM, Varaprasad K, Reddy GVS, Reddy AB, Sudhakar K, et al. Preparation and characterization of poly (ethylene glycol) stabilized nano silver particles by a mechanochemical assisted ball mill process. *J Appl Polym Sci* 2016; 133(7):123–36.
- Jyoti K, Baunthiyal M, Singh, A. Characterization of silver nanoparticles synthesized using *Urtica dioica* Lin. leaves and their synergistic effects with antibiotics. *J Radiat Res Appl Sci* 2016; 9(3):217–27.
- Kayalvizhi T, Ravikumar S, Venkatachalam P. Green synthesis of metallic silver nanoparticles using *Curculigo orchioides* rhizome extracts and evaluation of its antibacterial, larvicidal, and anticancer activity. *J Environ Eng* 2016; 142(9):C4016002.
- Kora AJ, Manjusha R, Arunachalam J. Superior bactericidal activity of SDS capped silver nanoparticles: synthesis and characterization. *Mater Sci Eng C* 2009; 29(7):2104–9.
- Kumar P, Pirjola L, Ketzler M, Harrison RM. Nanoparticle emissions from 11 nonvehicle exhaust sources—a review. *Atmos Environ* 2013; 67:252–77.
- Matai C, Sachdev A, Dubey PS, Kumar U, Gopinath PB. Antibacterial activity and mechanism of Ag–ZnO nanocomposite on *S. aureus* and GFP-expressing antibiotic resistant *E. coli*. *Colloids Surf B Biointerfaces* 2014; 115:359–67.
- Nagaonkar D, Rai M. Sequentially reduced biogenic silver-gold nanoparticles with enhanced antimicrobial potential over silver and gold monometallic nanoparticles. *Adv Mater Lett* 2015; 6(4):334–41.
- Nanocomposix. Nanocomposix's guide to dynamic light scattering (DLS) measurement and analysis. 2015. Available via <https://cdn.shopify.com/s/files/1/0257/8237/files/>

- nanoComposix_Guidelines_for_DLS_Measurements_and_Analysis.pdf? 13 2/2015
- Nanocomposix. UV/VIS/IR spectroscopy analysis of nanoparticles. 2012. Available via https://cdn.shopify.com/s/files/1/0257/8237/files/nanoComposix_Guidelines_for_UV-vis_Analysis.pdf?13692/2012
- Patil SS, Mali MG, Tamboli MS, Patil DR, Kulkarni MV, Yoon H, et al. Green approach for hierarchical nanostructured Ag-ZnO and their photocatalytic performance under sunlight. *Catal Today* 2016; 260:126–34.
- Pai, V., Chanu, T. R., Chakraborty, R., Raju, B., Lobo, R., & Ballal, M. (2011). Evaluation of the antimicrobial activity of Punica granatum peel against the enteric pathogens: An in vitro study. *Asian Journal of Plant Science and Research*, 1(2), 57-62.
- Shah AH, Manikandan E, Ahmed MB, Ganesan V. Enhanced bioactivity of Ag/ZnO nanorods—a comparative antibacterial study. *J Nanomed Nanotechnol* 2016; 4:168–73.
- Shahverdi AR, Minaeian S, Shahverdi HR, Jamalifar H, Nohi AA. Rapid synthesis of silver nanoparticles using culture supernatants of Enterobacteria: a novel biological approach. *Process Biochem* 2007; 42(5):919–23.
- Rao KJ, Paria S. Green synthesis of silver nanoparticles from aqueous Aegle marmelos leaf extract. *Mater Res Bull* 2013; 48(2):628–34.
- Taylor P, Ussher A, Burrell R. Impact of heat on nanocrystalline silver dressings: part I: chemical and biological properties. *Biomaterials* 2005; 26(35):7221–9.